Available online at www.sciencedirect.com
ScienceDirect
Acta Materialia 59 (2011) 554–562
Acta MATERIALIA
www.elsevier.com/locate/actamat

A continuous and one-to-one coloring scheme for misorientations

Srikanth Patala, Christopher A. Schuh *

Department of Materials Science and Engineering, Massachusetts Institute of Technology, Cambridge, MA 02139, USA

Received 3 August 2010; accepted 27 September 2010

Abstract

Grain boundaries and their networks have profound influence over properties and structure evolution in every class of polycrystalline materials. Despite recent advances in characterization techniques, there remain fundamental problems in representing grain boundary network information; existing methods neglect the full complexity of misorientation information and often rely on boundary classification schemes of dubious physical significance. This situation has arisen in part because grain boundary misorientations have no known mapping to a simple Euclidean space; conventional wisdom suggests that the misorientation space is equivalent to the rotation space, which is known to require five variables for a continuous one-to-one mapping. In this paper, we show that, contrary to this expectation, the misorientation spaces for homophase misorientations for the 432 point group can indeed be mapped to three-dimensional Euclidean space. With this advance, we show that grain boundary networks can now be "colored", with every color uniquely reflecting the full misorientation information of every boundary in the network.

Keywords: Misorientation; Topology; Misorientation mapping; EBSD; Coloring scheme

1. Introduction

The critical importance of grain boundary networks has long been known to materials scientists as providing, e.g. the backbone for intergranular damage processes [1], or the series of barriers to conductive transport, through polycrystals [2,3]. At the same time, the properties of grain boundaries have extremely high contrast, with some boundaries exhibiting properties orders of magnitude different from others in the same material. Revolutionary improvements in many material properties have been achieved through "grain boundary engineering", where the populations of some types of boundaries and their global connectivity have been manipulated [4]; some examples include a 50-fold increase in weldability [5], a 16-fold decrease in creep rate [6], a fourfold increase in service life of battery electrodes [7] and a sevenfold increase in critical current density in high-T_c superconductor $YBa_2Cu_3O_7$ [8].

Along with the increasing recognition that grain boundary types and their networks are key to structure–property connections [9], the materials community has developed an impressive suite of experimental tools to study them. From the earliest studies using manual mapping in the transmission electron microscope [10] to automated two-dimensional spatial orientation mapping by electron backscatter diffraction (EBSD) [11], to the present toolkit that includes three-dimensional X-ray diffraction [12] and automated serial sectioning methods [13], the field has progressed to the point where the materials scientist now has a quantitative view of the boundary network in full crystallographic detail [14,15]. However, the experimental capabilities of the field have outpaced our ability to interpret and represent the full boundary information. Existing methods always discard some misorientation information [4,16], and tend to classify boundaries into simplistic categories, e.g. as low vs. high-angle boundaries or high vs. low coincidence boundaries.

Fig. 1 shows some examples of these common methods of mapping grain boundary types, using an EBSD map of a

* Corresponding author.
E-mail address: schuh@mit.edu (C.A. Schuh).

1359-6454/$36.00 © 2010 Acta Materialia Inc. Published by Elsevier Ltd. All rights reserved.
doi:10.1016/j.actamat.2010.09.058

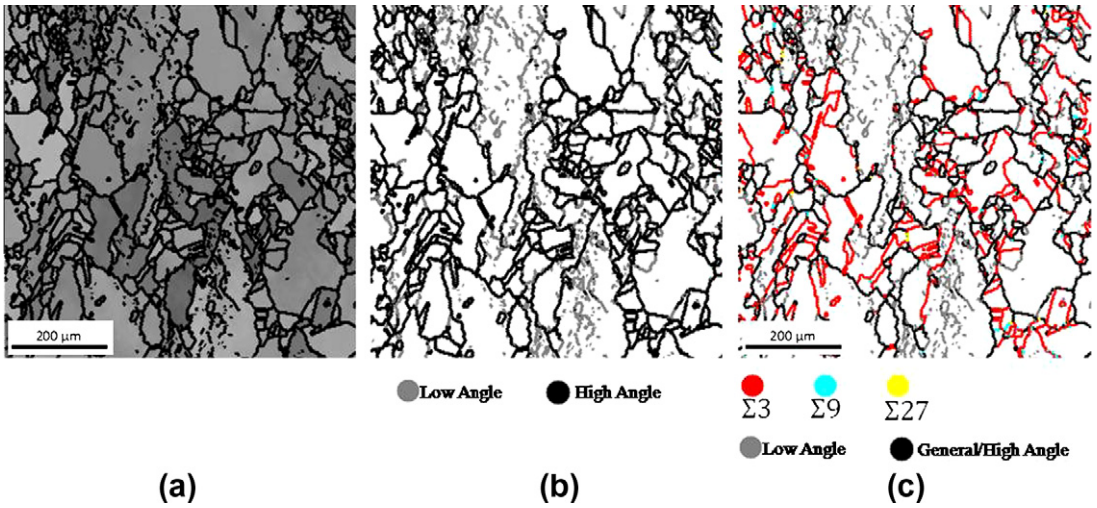

Fig. 1. Deficiencies in existing grain boundary maps. (a) Sample of a Cu–Cr alloy analyzed using EBSD, where grain boundaries are highlighted and each grain is shaded. (b) Grain boundaries colored according misorientation angle alone (low- vs. high-angle). (c) Grain boundary map showing the specific coincidence misorientations called Σ3 (red), Σ9 (light blue) and Σ27 (yellow), as well as low-angle (gray) and high-angle (black) boundaries. These maps do not represent complete misorientation information and the coloring does not capture misorientation distances between the various boundaries. (For interpretation of the references to color in this figure legend, the reader is referred to the web version of this article.)

specimen of a polycrystalline copper–chromium alloy. Fig. 1a shows the microstructure, with grains shaded in various grays and grain boundaries highlighted in black. Fig. 1b and c show the same dataset, with grain boundaries differentiated by categories based on misorientation: Fig. 1b classifies boundaries into low- and high-angle boundaries differentiated by shading, and Fig. 1c adds colors corresponding to some "special" misorientations corresponding to coincidence site lattice numbers Σ3, 9 and 27, which are prevalent in twinning materials. Both of these types of maps are common in the literature, and abandon most of the available misorientation information captured in the original EBSD dataset. Furthermore, these maps do not capture any *relative* misorientation information, that is, information regarding the "distance" between individual misorientations.

We suggest that the reason grain boundary networks are viewed with such rudimentary classification schemes is largely mathematical: the full spectrum of misorientations is not presented in such maps because there is no known method of doing so. The central goal of this paper is to present an unexpected mathematical discovery about misorientation spaces, which in turn leads to a new method of coloring grain boundary networks such as those shown in Fig. 1. We develop a method to label each boundary segment with a single color that uniquely (one-to-one) identifies its misorientation, with no part of the misorientation information neglected, and where similar misorientations have similar colors (continuous). Mathematically, we develop a continuous one-to-one mapping between the color space and the space of misorientations for crystals of 432 point symmetry, i.e. we illustrate the embedding of the 432-misorientation space in the color space.

2. The topology of misorientation spaces

The difficulty of establishing a mapping between misorientations and colors arises because of the apparent mismatch in topology between these two spaces. Color spaces, like the ones illustrated in Fig. 2, are *simply connected* [17] spaces in R^3, and are represented as, for example, a cube (the well-known red–green–blue or RGB space, Fig 2a), a solid ball (the so-called hue–saturation–lightness or HSL space, Fig. 2b) or a cone (the hue–saturation value or HSV space, Fig. 2c). On the other hand, rotation space is not simply connected and is of higher dimensionality [18]. Misorientations are usually considered as equivalent to rotations, i.e. the rotation required to bring crystal A into coincidence with a second crystal B, and rotation space can only be embedded in a Euclidean space with at least five dimensions (R^5) [19,20].

The topology of rotations is most easily illustrated by plotting the rotations in three dimensions as a parametric ball, as shown in Fig. 3a. This parametric ball is an axis–angle representation of rotations, that is, any given point in the parametric ball lies on the axis of rotation ($\vec{n}$), and sits at a radial position proportional to the rotation angle ω (out to the symmetry point for rotation angle of $\omega = \pi$). Every point in the solid ball represents a unique rotation except for the points on its surface. Each surface point corresponds to a rotation of π. And, since any rotation $(\vec{n}, \pi)$ is equivalent to the rotation $(-\vec{n}, \pi)$, the diametrically opposite surface points are identified, as illustrated in Fig. 4a. It is this equivalence of the antipodal points that makes the topology of rotations non-trivial and embedding in three Euclidian dimensions impossible. Thus, although the parametric ball in Fig. 3a and the HSL color ball in Fig. 2b have the same shape, they have fundamentally

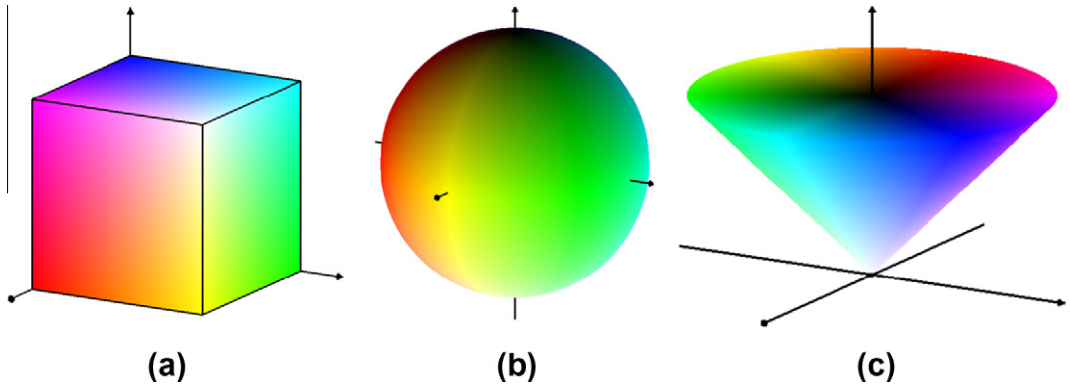

Fig. 2. Common representations of the color space. (a) RGB color space; (b) HSL color space; (c) HSV color space. Color spaces are simply connected in R^3. (For interpretation of the references to color in this figure legend, the reader is referred to the web version of this article.)

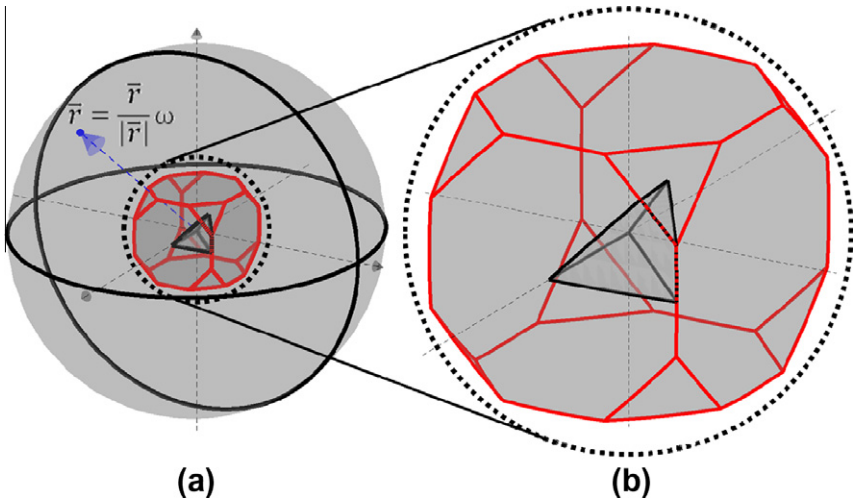

Fig. 3. The spaces of rotations, orientations and misorientations. (a) Parametric ball used to represent rotations in R^3. The point $\vec{r}$ represents a rotation of angle $|\vec{r}|$ through the axis $\frac{\vec{r}}{|\vec{r}|}$. Also shown in (b) are the 432-orientation and misorientation fundamental zones that form a part of the parametric ball.

different connectivity; if colors were assigned by naively fitting one to the other, nominally very similar rotations could exhibit large color differences.

Thus, it is an established fact that rotations cannot be embedded in three-dimensional Euclidean space, and it is widely believed that orientations and misorientations cannot be either. The spaces of orientations and misorientations are equivalent to the rotation space with additional equivalence relations that arise due to the point symmetries of crystals; this has the effect of partitioning the rotation space into symmetrically equivalent "fundamental zones", such as the well-known one shown in Fig. 3b for orientations in the cubic (432) system. However, crystal symmetries unfortunately do not remove the path discontinuities inherent to the rotation group, as shown by the dashed paths in Fig. 4b, which exhibit "jumps" where they pass through the boundaries of the zone.

We have found that an unexpected special situation arises when considering homophase misorientations among crystals of the 432 point group, fundamentally changing the character of the discontinuities illustrated for rotations and orientations in Fig. 4a and b. Moving from orientations to misorientations introduces significant additional symmetry (because two crystal symmetries are involved instead of one), and thus the misorientation space for this system (shown in Fig. 3b) is a subset of the cubic orientation space. However, beyond simply adding additional crystal symmetries, another special symmetry is introduced in the case of homophase boundaries [21]. Since the two adjoining grains that constitute a homophase grain boundary are physically indistinguishable [22], the misorientation observed in the reference frame of grain 1 ($\mathbf{M_{12}}$) is equivalent to the misorientation observed in the reference frame of grain 2 ($\mathbf{M_{21}} = \mathbf{M_{12}^{-1}}$). We refer to this as "grain exchange symmetry". We may write a set of equivalence relations that render all symmetric misorientations equivalent, including not only the rotational symmetry operations of the crystal point group (denoted $\mathbf{S_i}$ and $\mathbf{S_j}$), but also the grain exchange symmetry:

$$\mathbf{M_{12}} \sim \mathbf{M_{21}} \Rightarrow \mathbf{M} \sim \mathbf{M^{-1}} \Rightarrow \mathbf{M} \sim \mathbf{S_i M S_j} \sim \mathbf{S_j^{-1} M^{-1} S_i^{-1}} \qquad (1)$$

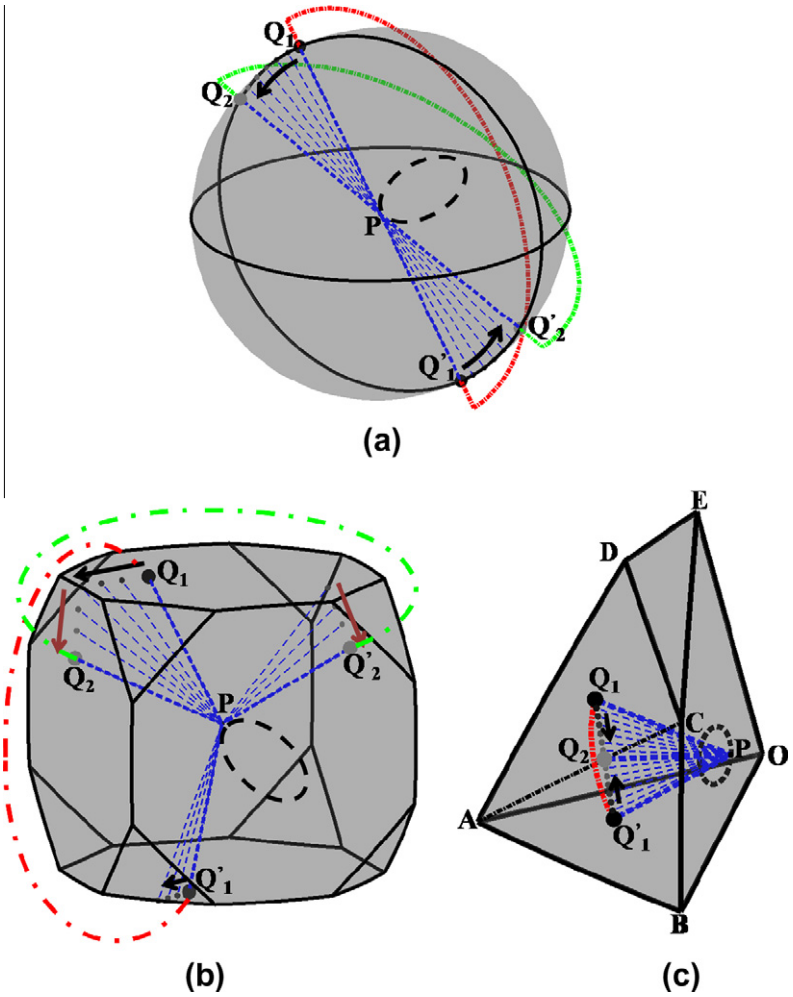

Fig. 4. Path connectivity and character of jumps in (a) rotation space, (b) 432-orientation space and (c) 432-misorientation space. The dashed black line represents a continuous path completely contained within the space. The dashed blue lines represent paths with a jump (shown using green and red dashed lines). (For interpretation of the references to color in this figure legend, the reader is referred to the web version of this article.)

The effect of this additional equivalence relation is examined by looking at the classes of the paths and, more importantly, their discontinuities or jumps, in the rotation, 432-orientation and 432-misorientation spaces. Two coterminous paths belong to the same class (are *homotopic*) if one can be continuously deformed into the other and vice versa. A construction similar to that of Wigner and Griffin [23] for the rotation space is used to examine the jumps in the orientation and misorientation spaces. Shown in Fig. 4a–c are paths of two kinds: one that comprises a jump (blue paths with colored jumps) and the other that is continuous and completely contained within the space (dashed black line). The character of the jumps is examined by continuously deforming the blue path. As shown in Fig. 4a, the initial path $PQ_1Q_1'P$ can be distorted continuously to a great extent, for example to the path $PQ_2Q_2'P$, but the two surface points that define the jump QQ' are always diametrically opposite; the jump can never be removed.

The jump in 432-orientation space has a similar character. When a path intersects the surface (Fig. 4b) at point Q it re-enters the space at a point that is obtained by rotating point Q through a certain angle and reflecting it onto the opposite surface Q'; this jump has a skewed character reminiscent of a Möbius strip [24]. No amount of distortion can remove the jump as the points Q, Q' are always on opposite faces of the orientation space.

In the case of 432-misorientation space, path discontinuities do not occur at the surfaces except for the surface $ABCD$ (Fig. 4c). When the paths hit the surface $ABCD$ they re-enter *through the same surface,* at a point obtained by reflecting through the line AC. As illustrated in Fig. 4c, this jump can be removed by continuously moving point Q onto the line AC; once the jump is removed, the path can be continuously distorted into any other path without a jump. From this we conclude that, unlike the rotation and orientation spaces, the 432-misorientation space is simply connected (i.e. has a trivial fundamental group).

The change in topology between the 432-orientation and misorientation spaces described above is not anticipated by conventional arguments about rotational point symmetries; grain exchange symmetry, $\mathbf{M} \sim \mathbf{M}^{-1}$, is crucial to this change in topology. If a heterophase boundary is

considered, this symmetry no longer applies and the misorientation space does not admit a trivial fundamental group. This is because groups containing only rotational symmetries act *properly discontinuously* [25] on the rotation space. In simple terms, this means that whenever a path intersects the surface of the fundamental zone of these spaces a jump occurs that cannot be removed by any amount of path distortion. On the other hand, the equivalence relation $\sim \mathbf{M}^{-1}$ alters the topology of some surfaces such that when a path intersects this surface it gets reflected back into the fundamental zone at the same point [26]. But the $\sim \mathbf{M}^{-1}$ relation alone is not a sufficient condition for an embedding in R^3, as the misorientation space must be simply connected. This condition can only be checked geometrically. We have performed this check for the 432 point group and find that the 432-misorientation space is indeed simply connected; this will be established more clearly in the next section. The simply connected criterion is justified through the famous Poincaré conjecture [27], which asserts that simply connected three-dimensional manifolds are homeomorphic to a 3-sphere (and any proper subset of a 3-sphere can be embedded in R^3).

3. Explicit mapping for the 432-misorientation space

To obtain a one-to-one continuous mapping for the 432-misorientation space into the color space, the former must be deformed continuously so that the path discontinuities are removed. We have developed such a mapping, as illustrated in Fig. 5, which shows a sequence of deformations that maps the 432-misorientation space into the shape of a cone, with no surfaces that induce path discontinuities. The cone shape was selected so that it can be directly fitted to the HSV color cone (see Fig. 2c) to obtain a coloring scheme for misorientations. The most critical of the deformation steps is the folding of the space shown in frames

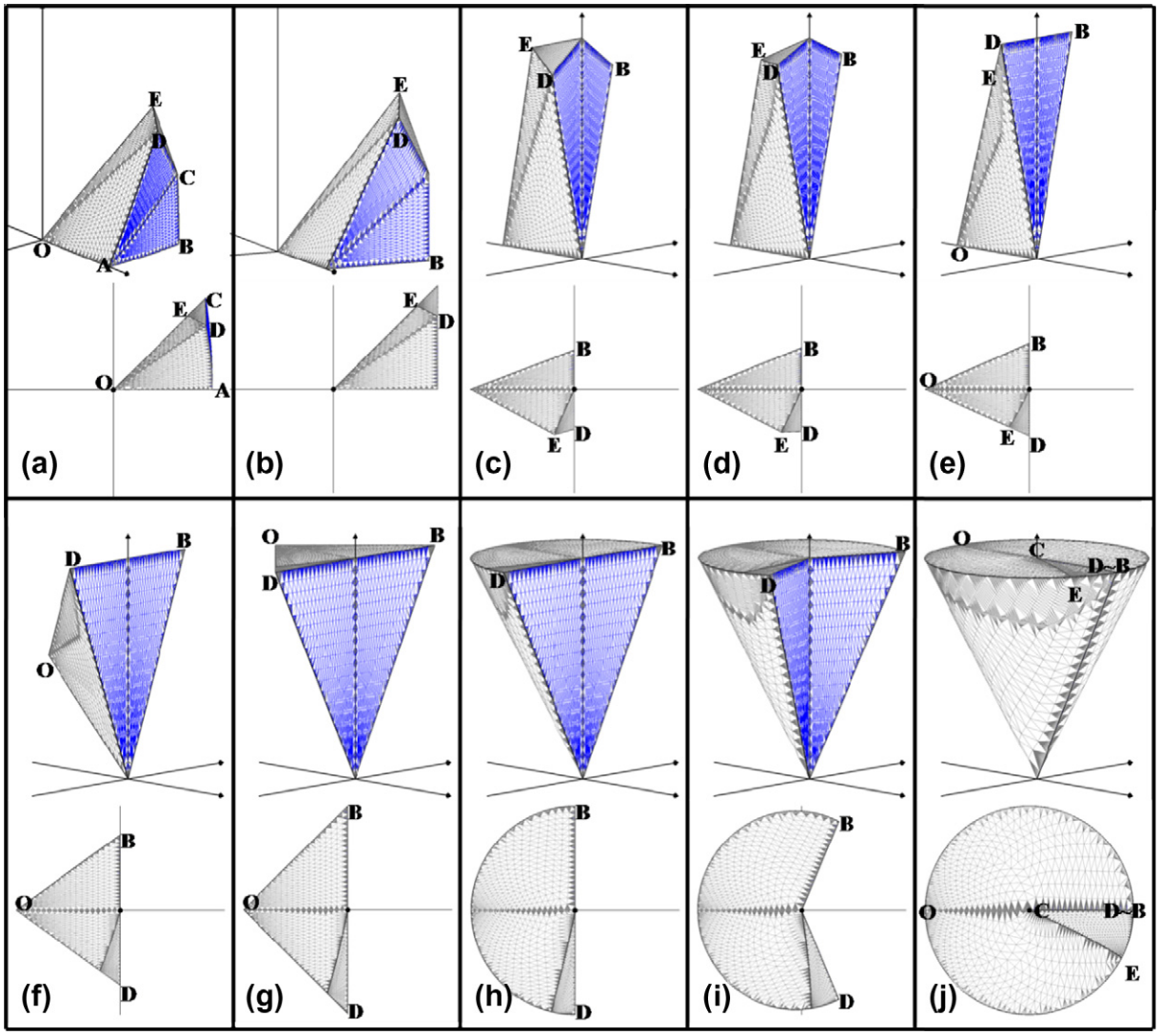

Fig. 5. Continuous deformation of the 432-misorientation space. (a) Axis–angle representation of 432-misorientation space (432-MS). (b) A continuous mapping into a Rodrigues-vector representation of 432-MS with straight edges and planes. (c–e) the same space subsequently rotated and surfaces flattened. (e–g) Continuous deformation of (e) into a prism. (g and h) A prism to a half-cone. (h–j) A half-cone to a cone. This deformation is an embedding of 432-MS in R^3 and the final cone obtained is a simply connected space in R^3.

Fig. 5h–j, which leads to the closure of the surface ABD upon itself in such a way that the path discontinuities are healed; the original two triangular planes ABC and ADC are glued together. The deformations shown graphically in Fig. 5 may also be expressed analytically as:

$$
\begin{aligned}
&(1)\quad (x,y,z) \equiv \left(n_x \tan\left(\frac{\omega}{2}\right),\quad n_y \tan\left(\frac{\omega}{2}\right),\quad n_z \tan\left(\frac{\omega}{2}\right)\right)\\
&(2)\quad (x_1,y_1,z_1) \equiv \begin{cases} \left(x, \frac{x(y+z)}{1-x}, \frac{xz(y+z)}{y(1-x)}\right) & \text{for } x \geqslant \frac{1}{3} \text{ and } \tan\left(\frac{z}{y}\right) \geqslant \left(\frac{1-2x}{x}\right) \\ (x,y,z) & \text{otherwise} \end{cases}\\
&(3)\quad |x_2,y_2,z_2\rangle \equiv g^* |x_1 - \tan\left(\frac{\pi}{8}\right),\quad y_1,z_1\rangle;\quad g = R\left([100], \frac{3\pi}{8}\right)\\
&\qquad \text{where } R(\omega,\bar{n}) \text{ represents a rotation of angle } \omega \text{ along the axis } \bar{n}.\\
&(4)\quad (x_3,y_3,z_3) \equiv \left(x_2, y_2\left(1+\frac{y_2}{z_2}\tan\left(\frac{\pi}{8}\right)\right),\quad z_2 + y_2 \tan\left(\frac{\pi}{8}\right)\right)\\
&(5)\quad (x_4,y_4,z_4) \equiv \left(x_3, \frac{y_3 \cos\left(\frac{\pi}{8}\right)}{\tan\left(\frac{\pi}{8}\right)},\quad z_3 - \frac{x_3}{\cos\left(\frac{\pi}{8}\right)}\right)\\
&(6)\quad (x_5,y_5,z_5) \equiv (x_4(\sin\phi + |\cos\phi|),\quad y_4(\sin\phi + |\cos\phi|), z_4);\\
&\qquad \phi = a\tan\left(-\frac{x_4}{y_4}\right)\\
&(7)\quad (h,s,v) \equiv \left(-\sqrt{x_5^2+y_5^2}\cos 2\phi_1,\quad \sqrt{x_5^2+y_5^2}\sin 2\phi_1,\quad z_5\right);\\
&\qquad \phi_1 = a\tan\left(-\frac{y_5}{x_5}\right)
\end{aligned}
\tag{2}
$$

With a misorientation described in axis–angle parameters as input to Eq. (2), the sequence of subsequent formulae returns a color in the HSV space.

4. Application to EBSD data

Eq. (2) may be used to construct a "color legend" in the 432-misorientation fundamental zone. This is shown in Fig. 6, where sections at constant intervals of disorientation angle of the 432-misorientation space from Fig. 3b are presented. The result is a sequence of sections that each resemble the standard stereographic triangle, with corners that lie on (1 0 0), (1 1 0) and (1 1 1); at large disorientation angles the triangle is truncated as the sectioning planes begin to exit the fundamental zone. Not only does the coloring scheme satisfy continuity and provide a unique color for every point in the space, but it has been constructed with several additional conveniences for intuitive interpretation. For example, the contrast maps generally to the disorientation angle: high-angle misorientations have darker colors and low angles correspond to lighter colors, with white being located at the apex ($\omega = 0$). Red, green and blue are located at important symmetry points on (1 0 0), (1 1 0) and (1 1 1) respectively, with blue corresponding to the twin misorientation of 60° on (1 1 1).

With the legend shown in Fig. 6, we may now create a grain boundary map that contains the complete misorientation information, mapped to colors via the transformation sequence in Eq. (2). An example of such a map is shown in Fig. 7, for the same set of EBSD data already presented in Fig. 1. The misorientation information can be directly inferred from the legend of Fig. 6 by matching the boundary color, reading the misorientation angle from the standard stereographic triangle in which it falls, and the misorientation axis from its position in the triangle. Comparing Fig. 7 to either of the two representations in Fig. 1 reveals the qualitative power of the new mapping; whereas Fig. 1 bins misorientations into classes and neglects most of the misorientation information, Fig. 7 involves no loss of information and covers the entire misorientation spectrum. The discovery of a continuous mapping of colors to misorientations also guarantees that boundaries of similar misorientation are colored similarly, and vice versa.

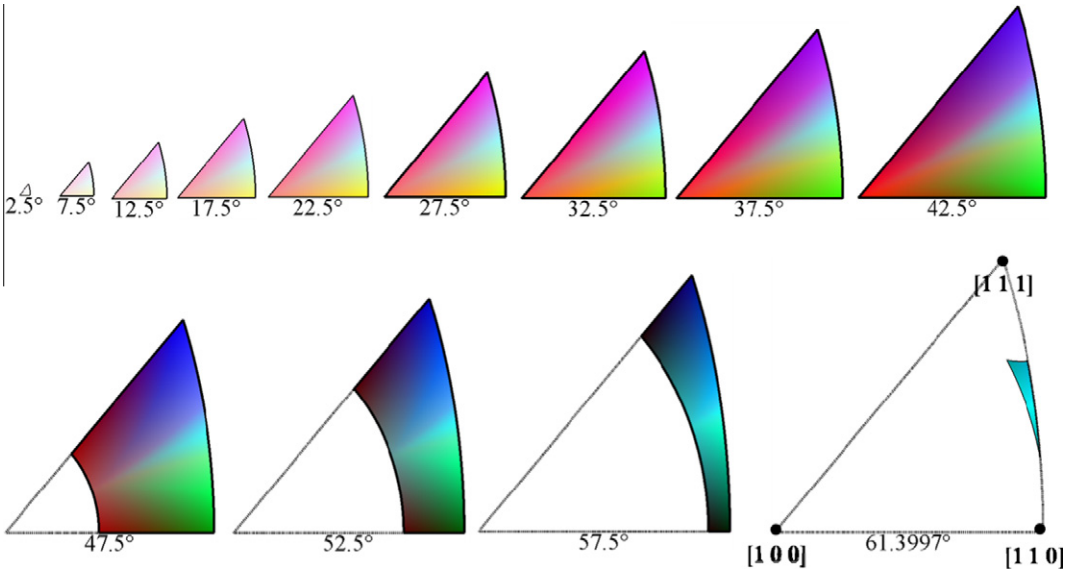

Fig. 6. Color legend for homophase misorientations, built using stereographic projection of surfaces of constant misorientation angle, ω. Each triangle is the well-known standard stereographic triangle. (For interpretation of the references to color in this figure legend, the reader is referred to the web version of this article.)

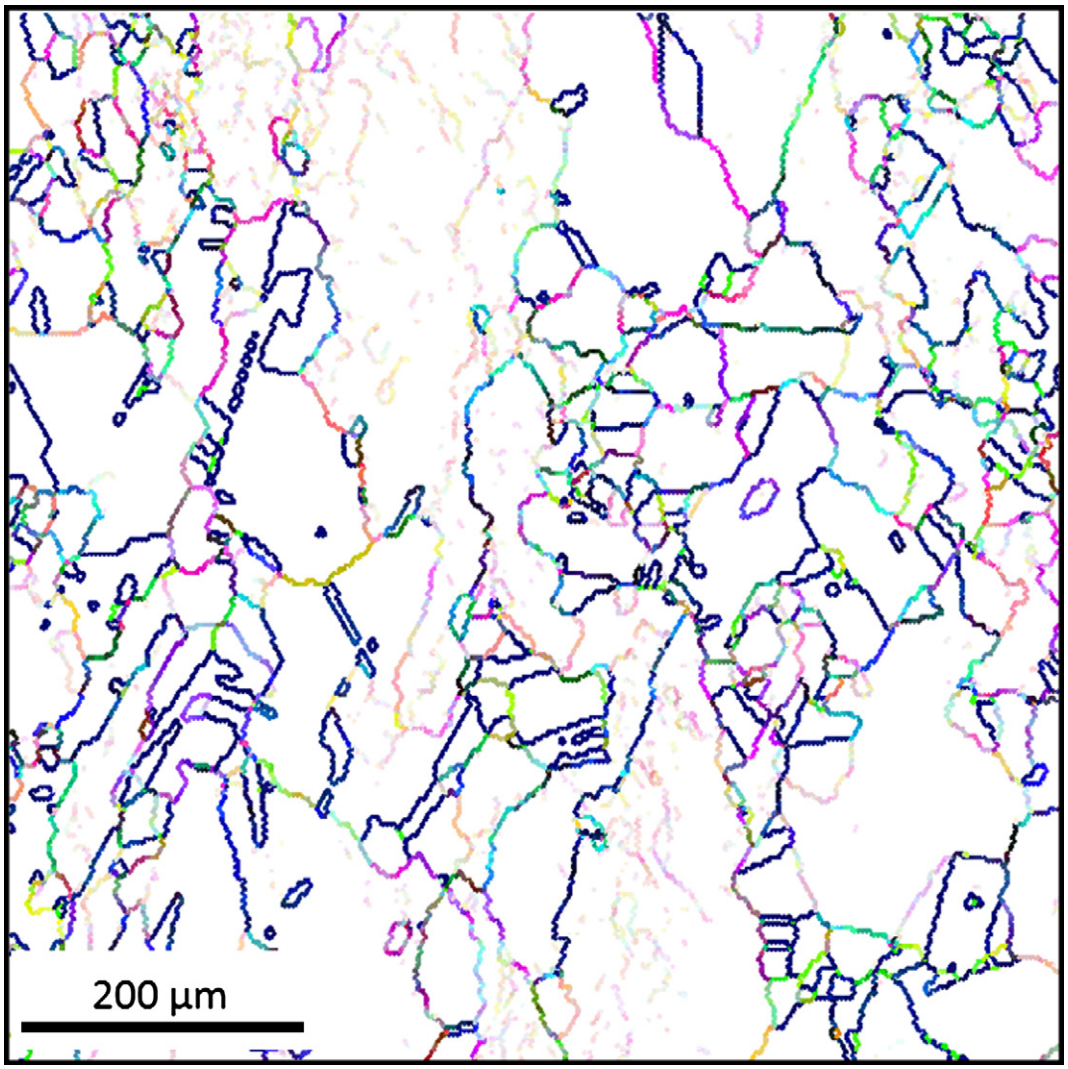

Fig. 7. Grain boundary misorientation map with a coloring scheme that is one-to-one and continuous. Complete misorientation information (axis and angle) can be directly interpreted using the legend in Fig. 6. Since the colors represent a continuous mapping, contrast in the colors represents misorientation distance. (For interpretation of the references to color in this figure legend, the reader is referred to the web version of this article.)

The mapping of 432-misorientation space to R^3 also has implications beyond the problem of coloring grain boundary maps. For example, the mapping of misorientations to three-dimensional Euclidean space can be used to develop better coloring schemes for the orientations of individual grains. Orientations lack much of the symmetry of misorientations, and occupy a larger space (see the red zone in Fig. 3b). As noted above, the 432-orientation space is not simply connected in three dimensions, so it is not formally possible to color orientations in a continuous and one-to-one manner. However, we may capture most of the orientation information using an approximation: grain orientations can be considered as misorientations with respect to a fixed reference frame. Given a grain orientation lying in the 432-orientation fundamental zone, additional crystal symmetries and the grain exchange symmetry can be applied to find its equivalent parameters in the misorientation fundamental zone and thus a color can be attributed. The caveat is that there are 48 distinct orientations that will be mapped to the same misorientation and hence will have the same color.

We apply this method to the coloring of grain orientations in Fig. 8a, which is the same set of EBSD data for Cu–Cr used throughout the paper. We choose a reference orientation aligned with the sample axes, and plot the grain color as the disorientation with respect to this reference frame. For comparison, shown in Fig. 8b are grain orientation maps using a more traditional inverse pole figure representation, with the legend shown in the inset. Whereas the map in Fig. 8b only contains information about the crystallographic vector normal to the viewing plane, the coloring scheme in Fig. 8a captures far more information over the misorientation space. For example, consider the grains circled in the lower right hand corner of Fig. 8. Whereas the grains are colored a very similar shade of yellow in Fig. 8b, they abut a grain boundary and are actually oriented very differently; they are misoriented by a rotation in the plane that is not captured by examination of the

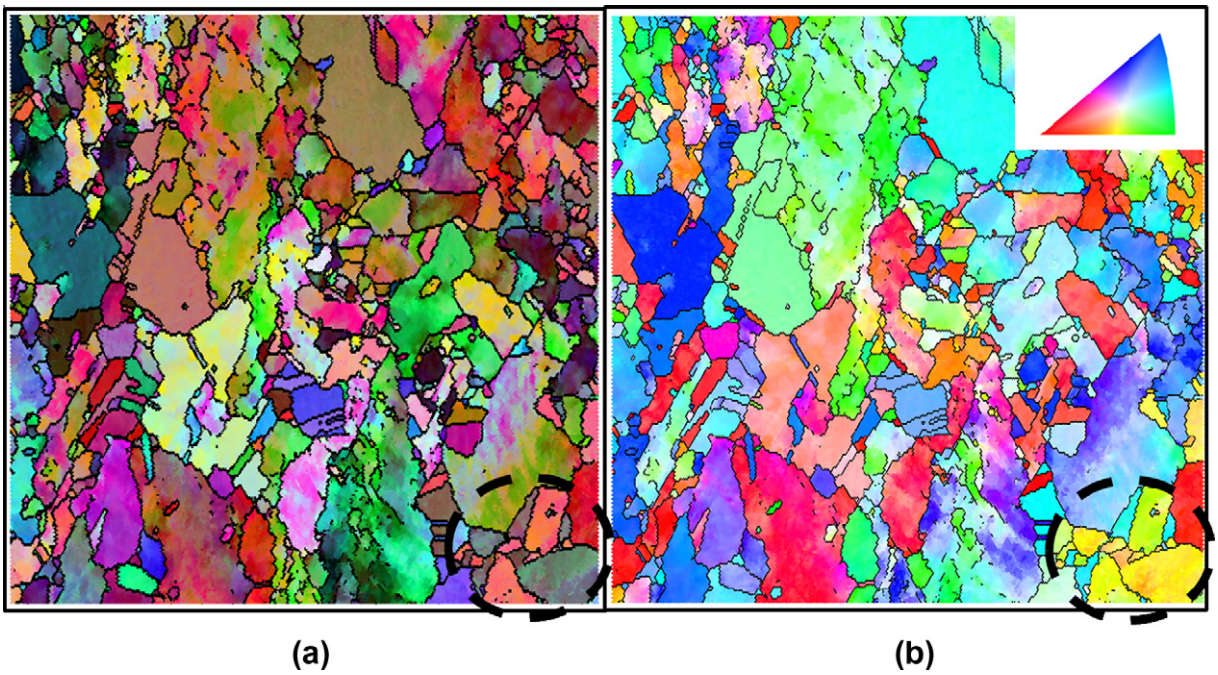

Fig. 8. Representations of EBSD data using colors to denote grain orientations. (a) Grain orientations colored according to misorientation with respect to the sample reference frame, using the legend from Fig. 6. (b) Grain orientations colored using traditional inverse pole figure representation, with the legend in the upper-right corner showing the mapping of color to surface normal vector. The grains in the dashed circle are used to show the advantages of this approximate coloring scheme using misorientations as compared to the inverse pole figure representation. (For interpretation of the references to color in this figure legend, the reader is referred to the web version of this article.)

surface normal vector alone. In contrast, this orientation difference is captured by the coloring scheme of Fig. 8a, which, by comparison to the legend in Fig. 6, reveals a large misorientation of 60°. Examination of the grain boundary map in Fig. 7 further emphasizes the point.

5. Conclusions

We have shown that the misorientation space for homophase misorientations among crystals with 432 point symmetry is simply connected in three Euclidean dimensions. This result is somewhat unexpected, since rotations and orientations are known to require more than three dimensions for a continuous and one-to-one representation. Our discovery here is a special case that arises for the homophase misorientations among 432 symmetric crystals. In this case the application of both crystal point symmetries and the "grain exchange symmetry" (i.e. the symmetry that arises because the reference frame of the misorientation may be used in either of the two grains) leads to a change in the topology of the space. We have demonstrated an continuous one-to-one mapping (an embedding) of the 432-misorientation space with R^3.

Our result has immediate practical application in the representation of misorientation data from, for example, electron backscatter diffraction, as it permits mapping of misorientations to colors with no loss of information. We have demonstrated the coloring of a grain boundary network in a specimen of copper as a proof of this concept. If a reference orientation is defined, the method also permits coloration of grain orientations in a new way that captures information lost in conventional "inverse pole figure" mapping common in the field.

The embedding of misorientation space in R^3 also opens the door to more nuanced views of how misorientations are related to one another: whereas the "distance" between two misorientations is complicated by discontinuous jumps in the misorientation space, when embedded in R^3 the removal of discontinuities permits simple Euclidean distance calculations. The simplification of misorientations through this mapping is also a useful first step towards the development of a system for understanding the full five-parameter space of grain boundaries that includes the plane normal vectors [14], the topology of which is presently unknown. Finally, we note that, although here we have used a simple two-dimensional example to illustrate the coloring of grain boundary misorientations, the technique should naturally apply to more sophisticated three-dimensional datasets and computer simulations.

Acknowledgement

This work was supported by the US National Science Foundation under Contract DMR-0855402.

References

[1] Gertsman VY, Tangri K. Acta Mater 1997;45:4107–16.

[2] Babcock SE, Vargas JL. Annu Rev Mater Sci 1995;25:193–222.
[3] Maier J. Nat Mater 2005;4:805–15.
[4] Randle V. Mater Sci Technol 2010;26:253–61.
[5] Lehockey EM, Palumbo G, Lin P. Metall Mater Trans A 1998;29:3069–79.
[6] Lehockey EM, Palumbo G. Mater Sci Eng, A 1997;237:168–72.
[7] Lehockey EM, Limoges D, Palumbo G, Sklarchuk J, Tomantschger K, Vincze A. J Power Sources 1999;78:79–83.
[8] Norton DP, Goyal A, Budai JD, Christen DK, Kroeger DM, Specht ED, et al. Science 1996;274:755–7.
[9] Holm EA, Duxbury PM. Scripta Mater 2006;54:1035–40.
[10] Von Heimendahl M, Bell W, Thomas G. J Appl Phys 1964;35:3614.
[11] Adams BL, Wright SI, Kunze K. Metall Mater Trans A 1993;24:819–31.
[12] Jensen DJ, Lauridsen E, Margulies L, Poulsen HF, Schmidt S, Sørensen HO, et al. Mater Today 2006;9:18–25.
[13] Saylor DM, Morawiec A, Rohrer GS. Acta Mater 2003;51:3663–74.
[14] Rohrer GS, Saylor DM, El Dasher B, Adams BL, Rollett AD, Wynblatt P. Z Metallkd 2004;95:197–214.
[15] Rohrer GS, Randle V, Kim C, Hu Y. Acta Mater 2006;54:4489–502.
[16] Schuh CA, Kumar M, King WE. Acta Mater 2003;51:687–700.
[17] Munkres JR. Topology. Englewood Cliffs, NJ: Prentice Hall; 2000.
[18] Altmann SL. Rotations, quaternions, and double groups. Oxford: Clarendon Press; 1986.
[19] Hopf H. Vjschr. Naturf Ges Zurich 1940;85:165–77.
[20] Stuelpnagel J. Siam Rev 1964;6:422–30.
[21] Grimmer H. Acta Crystall A: Cryst Phys, Diffract Theor Gen Crystall 1974;30:685–8.
[22] Heinz A, Neumann P. Acta Crystallogr A 1991;47:780–9.
[23] Wigner EP, Griffin JJ. Group theory and its application to the quantum mechanics of atomic spectra. New York: Academic Press; 1959.
[24] Frank FC. Metall Mater Trans A 1988;19:403–8.
[25] Bredon GE. Topology and geometry. New York: Springer; 1997.
[26] Grimmer H. Acta Crystall A: Cryst Phys, Diffract Theor Gen Crystall 1980;36:382–9.
[27] Mackenzie D. Science 2006;314:1848–9.